


Interplay of femtoscopic and charge-balance correlations

Scott Pratt  and Karina Martirosova

Department of Physics and Astronomy and Facility for Rare Isotope Beams, Michigan State University, East Lansing, Michigan 48824, USA

 (Received 29 January 2022; accepted 18 April 2022; published 16 May 2022)

Correlations driven by the constraints of local charge conservation have been shown to provide insight into the chemical evolution and diffusivity of the high-temperature matter created in ultrarelativistic heavy ion collisions. Two-particle correlations driven by final-state interactions have allowed the extraction of critical femtoscopic space-time information about the expansion and dissolution of the same collisions. Whereas correlations from final-state interactions mainly appear at small relative momenta, a few tens of MeV/ c , charge-balance correlations extend over a range of hundreds of MeV/ c . In nearly all previous analyses, this separation of scales is used to focus solely on one class or the other. The purpose of this study is to quantitatively understand the degree to which correlations from final-state interactions distort the interpretation of charge-balance correlations and vice versa.

DOI: [10.1103/PhysRevC.105.054906](https://doi.org/10.1103/PhysRevC.105.054906)

I. INTRODUCTION

Charge balance correlations are rather simple to understand. For each observed charge, there exists either an additional opposite charge or one fewer charge of the same sign. Because charge is locally conserved, the balancing charge should be found nearby in coordinate space, and because of collective flow, this correlation is mapped onto relative momentum. A charge balance function (BF) binned by relative rapidity and relative azimuthal angle describes the probability of finding the balancing charge at some relative rapidity, Δy , and relative angle $\Delta\phi$:

$$\begin{aligned}
 & B(\Delta y, \Delta\phi) \\
 &= \int d\phi_1 d y_1 d\phi_2 d y_2 \delta(y_1 - y_2 - \Delta y) \delta(\phi_1 - \phi_2 - \Delta\phi) \\
 &\quad \times \left\{ \frac{1}{2N_+} [P_{-+}(\phi_1, y_1; \phi_2, y_2) - P_{++}(\phi_1, y_1; \phi_2, y_2)] \right. \\
 &\quad \left. + \frac{1}{2N_-} [P_{+-}(\phi_1, y_1; \phi_2, y_2) - P_{--}(\phi_1, y_1; \phi_2, y_2)] \right\}, \\
 & N_{\pm} = \int d\phi dy P_{\pm}(\phi, y). \tag{1}
 \end{aligned}$$

The like-sign subtraction effectively identifies the location of the balancing charge on a statistical basis. Thus, $B(\Delta y, \Delta\phi)$ represents the conditional probability density for finding a balancing charge (either an opposite charge or the lowered chance of observing a charge of the same sign) separated by $\Delta\phi$ and Δy given the observation of a charge somewhere in the detector. BFs can also be indexed by hadron species, $B_{h|h'}(\Delta y, \Delta\phi)$. This then describes the probability of first observing a hadron species h' or \bar{h}' , then finding a particle of opposite charge of species h or \bar{h} . Due to the experimental difficulty in identifying hadrons which have decayed, the choice

of h and h' is often confined to pions, kaons, protons, and their antiparticles.

Even if two balancing charges are emitted from nearly the same point in coordinate space, they will separate in momentum space due to thermal motion. This separation in momentum space would be of the order of a few hundred MeV/ c , or equivalently $\lesssim 0.5$ radians or units of rapidity. If the balancing charges were created early and had the opportunity to diffuse far from one another in coordinate space, their final separations in momentum space might extend to twice that amount. The mean width of the BF, $\langle\Delta\phi\rangle$ or $\langle\Delta y\rangle$, i.e., the average separation of balancing charges, provides insight into the diffusivity or of the chemical evolution. Because $\langle\Delta y\rangle$ is relatively more sensitive to whether the particles were created early than $\langle\Delta\phi\rangle$ [1], one can constrain both the chemistry and diffusivity by BFs by analyzing BFs in terms of both Δy and $\Delta\phi$ [2–4]. This sensitivity is amplified by considering BFs indexed by hadronic species. For example, because strangeness is largely produced early in the collisions, kaon BFs, $B_{K|K}(\Delta\phi, \Delta y)$, are especially useful for extracting the diffusivity [4]. Numerous varieties of BFs have now been measured in heavy-ion collisions both by the STAR Collaboration at the Relativistic Heavy Ion Collider (RHIC) [5–14] and by the ALICE Collaboration at the Large Hadron Collider (LHC) [15–21]. At lower energies, the NA49 Collaboration has also measured BFs at CERN Super Proton Synchrotron (SPS) energies [22,23]. Detailed theoretical models describing the dynamics of charge correlations, superimposed onto state-of-the-art dynamical descriptions of the bulk evolution, have been able to quantitatively reproduce several features of measurements at both RHIC and the LHC [4,24–26]. The inferred diffusivity and chemistry from comparing models to data appears consistent with expectations from lattice gauge theory [27–29].

Correlations at small relative momentum are dominated by the effects of final-state interactions (FSI). The correlations

provide detailed spatial and geometric information describing the emission of final-state hadrons. Analyses of this class of correlations is often referred to as femtoscopy. Femtoscopic correlations are typically predicted through the Koonin formula [30,31],

$$C_{ab}(\vec{p}_a, \vec{p}_b) \equiv \frac{N_{ab}(\vec{p}_a, \vec{p}_b)}{N_a(\vec{p}_a)N_b(\vec{p}_b)} \approx \int d^3r S_{ab}(\vec{p}_a, \vec{p}_b, \vec{r}) |\phi(\vec{q}', \vec{r})|^2, \\ S_{ab}(\vec{p}_a, \vec{p}_b, \vec{r}) = \frac{\int d^4r_a d^4r_b s_a(r_a, \vec{p}_a) s_b(r_b, \vec{p}_b) \delta(\vec{r} - \vec{r}'_a + \vec{r}'_b)}{\int d^4r_a d^4r_b s_a(r_a, \vec{p}'_a) s_b(r_b, \vec{p}_b)}. \quad (2)$$

Here, $s_a(r, \vec{p})$ describes the probability of emitting a hadron of type a from space-time point r with momentum \vec{p} , and $\phi(\vec{q}, \Delta\vec{r})$ is the outgoing wave function for two particles with relative separation \vec{r} and relative momentum $\vec{q} = (\vec{p}_1 - \vec{p}_2)/2$, as measured in the center-of-mass of the pair frame. The primed coordinates represent the positions of emission in that frame. The function $S_{ab}(\vec{r})$ represents the probability that two particles, one of type a and one of type b , are emitted at points separated by \vec{r} in the two-particle center-of-mass frame. It is often referred to as the “source function,” though that is a misnomer because it does not represent the probability density of the emission function. More accurately, if you assume \vec{q}' is small, its dependence on \vec{r} represents the probability that two particles moving with the same velocity in the asymptotic state would be separated by \vec{r} . Generally, the goal of femtoscopic analyses is to extract information about $S_{ab}(\vec{r})$ from measurements of $C_{ab}(\vec{q})$.

There are variants of this formula, but they tend to all become equal in the limit that \vec{q} is small [32]. The correlation would be unity if the relative wave function were that of a plane wave, but, due to final-state interactions and symmetrization of the outgoing wave function, $|\phi(\vec{q}, \vec{r})|^2$ differs from unity and provides a correlation which is stronger when the relative positions, \vec{r} , are smaller. Thus, one gains insight into the spatial extent of $s(r, \vec{p})$. For identical pions, the wave function is symmetrized. If one neglects the Coulomb and strong interaction between the pions the squared wave function is then

$$|\phi(\vec{q}, \vec{r})|^2 = 1 + \cos(2\vec{q} \cdot \vec{r}), \quad (3)$$

and one can Fourier transform the correlation function to determine the source function, as long as one assumes that there is little dependence of S_{ab} on q . One could then extract both size and shape information about $S_{ab}(\vec{r})$.

The space-time characteristics of the emission provide insight into the equation of state [33,34]. For example, if the equation of state is soft, the expansion is slow and there is an evaporative nature to the emission. In that case, two pions of identical velocity, \vec{v} , might be separated by a large distance due to one pion being emitted early and the other coming late. The spatial separation is large along the direction of \vec{v} , while being more compact in the other directions. A more explosive source would result in a more compact spread. Further, for pions with higher velocity, compared to the expansion

velocity, emission is increasingly confined to the surface of the expanding fireball. This results in source sizes that fall with increasing transverse momentum [35].

Femtoscopic correlations are driven by three types of FSI: symmetrization or antisymmetrization of wave functions of identical particles, strong interaction, and Coulomb repulsion. Symmetrization effects extend out to relative momenta of $1/R$, where $R \approx 5$ fm is a typical characteristic size. This contribution to the correlation largely vanishes for $|\vec{q}| \gtrsim 50$ MeV/c. Strong interactions at low relative momentum are especially important because of the reduced phase space of the background. The two-proton correlation function has a peak at $q \approx 22$ MeV/c. The effect of strong interactions at higher relative momentum tends only to appear for well defined resonances, but those resonances, unlike the pp peak at $q \approx 22$ MeV/c, are typically included in BF analyses. The third class of FSI derives from the Coulomb interaction. For the Coulomb interaction the correlation extends to larger relative momentum, because the squared wave function behaves as $1 \pm me^2/q^2R$ at larger q . This is small due to the factor e^2 , but it becomes the dominant source of FSI at large q . Compared to correlation functions, BFs have an extra factor describing the background probability of observing a particle in the bin. If binning by the magnitude of the relative momentum, Q_{inv} , this factor grows quadratically with Q_{inv} due to phase space. Thus, compared to correlations functions, at least visually, BFs tend to magnify the strength of the Coulomb tail. Thus, special care must be given to Coulomb correlations when considering the effects of FSI on BFs. This includes accounting for the fact that any charged particle is accompanied by an oppositely charged balancing particle, which effectively screens the Coulomb interaction with third bodies [36].

A fourth type of interaction affects both charge-balance and femtoscopic correlations. That is annihilation. Within the context of a BF, annihilation is simply a negative source for pair creation. This leads to a dip in the BF at small relative momentum. However, if the annihilation involves particles, e.g., a proton and an antiproton that would not have interacted with other particles had they annihilated, the annihilation might have been considered as part of the final-state interaction wave function. For example, Eq. (2) could employ a relative wave function calculated from a complex optical potential [37,38]. In optical models of elastic scattering, the imaginary part of the potential accounts for the absorption, i.e., the inelastic channels. Here, that component would account for the annihilation of $p\bar{p}$ into mesons. Accounting for annihilation is complicated by the fact that particles can be regenerated. That is, if a baryon and antibaryon can decay to five hadrons, five hadrons can combine to form a baryon-antibaryon pair [39–42]. At chemical equilibrium, the rate and the inverse rates are equal. But, at final breakup, chemical equilibrium no longer holds and annihilation is more prevalent. Given the complexity and difficulty of including annihilation, it will not be considered in this paper, but instead is being pursued in a separate study.

Femtoscopic correlations are constructed to be dimensionless quantities, whereas BFs have units of density per unit rapidity, relative angle, or relative momentum. This comes from the fact that Eq. (2) has two powers of $N_i(\vec{p})$ in the

denominator whereas the definition of BFs in Eq. (1) has one power. The next section describes how charge-balance correlations and femtoscopic correlations are related.

The basic theory of charge balance calculations is reviewed in Sec. III while Sec. IV presents algorithm for calculating BFs from a blast-wave calculation. The theory and method for accounting for the screening of Coulomb interactions is presented in Sec. V. Results of calculations illustrating how correlations from FSI distort BFs are given in Sec. VI while Sec. VII shows how femtoscopic correlations at small relative momentum are affected by charge balance correlations. A summary, Sec. VIII, is followed by two Appendices, reviewing classical Coulomb correlations and the blast-wave fitting procedure respectively.

II. RELATING CHARGE-BALANCE AND FEMTOSCOPIC CORRELATIONS

Femtoscopic correlations are nearly always analyzed as a function of relative momentum. Typically, the range of relative momentum under consideration is $0 < q \lesssim 100$ MeV/c. By focusing on small relative momentum, one can better justify the approximation that the particles interact mainly with one another between the last interaction and the detector. In contrast, BFs are usually analyzed as a function of relative rapidity or relative azimuthal angle. They are sometimes binned by relative momentum, in which case the range of relative momenta tends to be in the range of several hundreds of MeV/c, which is the range of the thermal smearing of the space-time correlations.

Whereas femtoscopic correlations are constructed by dividing the two-particle distribution by an uncorrelated two-particle distribution, BFs are created by dividing by one single-particle distribution. Thus, BFs can be thought of as a ‘‘conditional distribution’’; i.e. given the observation of a charge, what is the probability of finding more charges of the opposite sign than of the same sign as a function of relative rapidity or relative azimuthal angle? The two forms are related by factors of the multiplicity,

$$B(p_1|p_2) = \frac{1}{2}C_{+-}(p_1, p_2)\frac{dN_+}{dp_1} + \frac{1}{2}C_{-+}(p_1, p_2)\frac{dN_-}{dp_1} - \frac{1}{2}C_{++}(p_1, p_2)\frac{dN_+}{dp_1} - \frac{1}{2}C_{--}(p_1, p_2)\frac{dN_-}{dp_1}. \quad (4)$$

The variables p_1 and p_2 could be any measure of the momentum. As an example, to obtain BFs binned by relative rapidity, p_2 might refer to any momentum in the detector and p_1 could refer to the relative rapidity. The quantity dN_{\pm}/dp_1 would then represent the number of charges of type \pm that would have the desired relative rapidity in a single event in the absence of correlation.

Similarly, one can generate correlation functions from BFs, but only the differences between same-sign and opposite-sign correlations, and only for the case that the correlations are unchanged if positive and negative particles are switched, i.e.,

$C_{+-} = C_{-+}$ and $C_{++} = C_{--}$. In that case

$$C_{\text{opp. sign}}(p_1, p_2) - C_{\text{same sign}}(p_1, p_2) = \frac{2B(p_1|p_2)}{dN_-/dp_1 + dN_+/dp_1}. \quad (5)$$

For a cylindrically symmetric boost-invariant distribution, which will be assumed throughout this paper, one can derive simple relations when the BF is binned by Δy , $\Delta\phi$, or Q_{inv} :

$$\begin{aligned} B_{h|h'}(\Delta y) &= \left(\frac{dN_{h+}}{dy} + \frac{dN_{h-}}{dy} \right) \\ &\quad \times [C_{h,h',\text{opp. sign}}(\Delta y) + C_{h,h',\text{same sign}}(\Delta y)], \\ B_{h|h'}(\Delta\phi) &= \frac{2Y_{\text{max}}}{\pi} \left(\frac{dN_{h+}}{dy} + \frac{dN_{h-}}{dy} \right) \\ &\quad \times [C_{h,h',\text{opp. sign}}(\Delta\phi) + C_{h,h',\text{same sign}}(\Delta\phi)], \\ B_{h|h'}(Q_{\text{inv}}) &= 2Y_{\text{max}}P_{h,h'}(Q_{\text{inv}}) \left(\frac{dN_{h+}}{dy} + \frac{dN_{h-}}{dy} \right) \\ &\quad \times [C_{h,h',\text{opp. sign}}(Q_{\text{inv}}) + C_{h,h',\text{same sign}}(Q_{\text{inv}})]. \end{aligned} \quad (6)$$

Here, Y_{max} is the range of the acceptance in rapidity, $-Y_{\text{max}} < y < Y_{\text{max}}$. The expressions are built on the assumption that the correlation functions are corrected for the acceptance in rapidity, meaning that, for any charge with rapidity y_1 , all charges with rapidities y_2 within the range of $y_1 - 2Y_{\text{max}} < y_2 < y_1 + 2Y_{\text{max}}$ are assumed to have been measured. The dependence on Y_{max} is especially important for $B_{h|h'}(\Delta\phi)$. If one were to increase the range in rapidity the correlations binned by $\Delta\phi$ would be diluted as would the charge balance functions. As long as correlations in Q_{inv} and Δy do not extend beyond $2Y_{\text{max}}$, $B(Q_{\text{inv}})$ and $B(\Delta y)$ are largely independent of Y_{max} . Here, Δy and $\Delta\phi$ refer to the absolute values of relative rapidity and relative azimuthal angle. Otherwise, the first two expressions in Eq. (6) would include an extra factor of $1/2$, and the remaining half the strength would be found at negative values of Δy and $\Delta\phi$. The relative momentum Q_{inv} is the magnitude of the relative momentum, $|\vec{p} - \vec{p}'|$, in the frame of the pair. Finally, $P_{h,h'}(Q_{\text{inv}})$ refers to the probability density of any two particles being separated by Q_{inv} , where the second particle is randomly boosted so that its rapidity is uniformly found in rapidity acceptance as described above. Because $P_{h,h'}$ will fall inversely with Y_{max} , the product $Y_{\text{max}}P_{h,h'}(Q_{\text{inv}})$ in the expression for $B_{h|h'}(Q_{\text{inv}})$ in Eq. (6) is independent of Y_{max} once Y_{max} is large enough to capture all the pairs for the specific Q_{inv} .

III. REVIEW OF CHARGE BALANCE CORRELATIONS

A hadron of type h with charge q_{hu} , q_{hd} , and q_{hs} (where u, d, s refers to the up, down, and strange charges) must be accompanied by balancing charges, carried by the altered distributions of other hadrons. Here, we show what number of hadrons $\delta N_{h'}$ result from the existence of δN_h . This is

represented by $\kappa_{h'|h}$, where

$$\delta N_{h'} = \kappa_{h'|h} \delta N_h. \quad (7)$$

First, we express $\delta N_{h'}$ in terms of a small chemical potential for a thermal system. We find the three chemical potentials, μ_u , μ_d , and μ_s , necessary to produce the correct amount of balancing charge. The number of hadrons of species h' is altered by the presence of a hadron h according to

$$\delta N_{h'} = \langle N_h \rangle \frac{\mu_a q_{h'a}}{T}, \quad (8)$$

where q_{ha} is the charge of type a on a hadron of type h , with $a = u, d, \text{ or } s$. This is a thermal argument where the number of hadrons of a species h' is altered by a factor $e^{\mu_a q_{h'a}/T} \approx 1 + \mu_a q_{h'a}/T$.

Summing over all the charges from all the hadrons h' should yield the charge that balances that carried by h ,

$$\begin{aligned} -q_{ha} &= \sum_{h'} \delta N_{h'} q_{h'a} = \sum_{h'} \langle N_{h'} \rangle \frac{\mu_b}{T} q_{h'b} q_{h'a} \\ &= V \chi_{ab} \frac{\mu_b}{T}, \quad \frac{\mu_a}{T} = -\frac{1}{V} \chi_{ab}^{-1} q_{hb}. \end{aligned} \quad (9)$$

Here, the charge susceptibility of a noninteracting gas is

$$\chi_{ab} = \frac{1}{V} \langle Q_a Q_b \rangle = \sum_h \langle n_h \rangle q_{ha} q_{hb}, \quad (10)$$

or, equivalently, the charge correlation for a noncorrelated hadron gas is confined to charges within the same hadron. This then provides the altered number of hadrons of type h' due to the existence of a single hadron of type h ,

$$\begin{aligned} \delta N_{h'} &= -\sum_{ab} \chi_{ab}^{(-1)} \langle n_{h'} \rangle q_{h'a} q_{hb}, \\ &= \kappa_{h'|h} \delta N_h, \\ \kappa_{h'|h} &= -\langle n_{h'} \rangle \sum_{ab} \chi_{ab}^{-1} q_{h'a} q_{hb}. \end{aligned} \quad (11)$$

Here, $\langle n_h \rangle$ is the mean density of hadrons of type h . The kernel $\kappa_{h'|h} = -\kappa_{h'|\bar{h}}$ because h and its antiparticle \bar{h} have opposite charges. Thus, for any BF,

$$\int d p' B_{h'|h}(p'|p) = \frac{1}{4} [\kappa_{h'|h} + \kappa_{h'|\bar{h}} - \kappa_{h'|\bar{h}} - \kappa_{\bar{h}'|h}]. \quad (12)$$

One can quickly check to see that if one were to sum the normalizations over all h' multiplied by $q_{h'a}$, one would indeed

find the charge q_{ha} :

$$\begin{aligned} &\sum_{h'} q_{h'a} \int d p' B_{h'|h}(p'|p) \\ &= \frac{1}{4} \sum_{h'} q_{h'a} [\kappa_{h'|h} + \kappa_{h'|\bar{h}} - \kappa_{h'|\bar{h}} - \kappa_{\bar{h}'|h}] \\ &= \sum_{h'} \sum_h q_{h'a} \langle n_{h'} \rangle q_{h'a} \chi_{a'b}^{-1} q_{hb} \\ &= \chi_{aa'} \chi_{a'b}^{-1} q_{hb} \\ &= q_{ha}. \end{aligned} \quad (13)$$

The expressions above ignore decays. Decays can be included by altering the kernels $\kappa_{h'|h}$ to include both the contribution where h' and h come from the same decaying parent, and the case where two charges correlated as described by the kernel κ above then decay to h' and h . If a hadron H decays into a set of channels c_H , where each channel has a branching ratio b_{c_H} , and if the number of hadrons of type h coming from the particular channel is m_{c_H} , the contribution to the kernel $K(h'|h)$ from decays is

$$\begin{aligned} K_{h'|h}^{(d)} &= \frac{1}{\langle \langle N_h \rangle \rangle} \sum_H \langle N_H \rangle b_{c_H} m_{c_H, h} m_{c_H, h'}, \\ \langle \langle N_h \rangle \rangle &= \sum_{H, c_H} \langle N_H \rangle m_{c_H, h} b_{c_H}. \end{aligned} \quad (14)$$

The channels c_H include the case where a particle is stable, i.e., where $H = h$ and there are no additional products. The notation $\langle \langle N_h \rangle \rangle$ signifies that this is the multiplicity after decays have taken place, whereas $\langle N_h \rangle$ signifies the density at the time hadrons were created with balancing charge assigned according to the arguments above.

One can then add in the contribution from correlations from charge balance at hadronization to find the complete kernel, K :

$$\begin{aligned} K_{h'|h} &= K_{h'|h}^{(d)} + \frac{1}{\langle \langle N_h \rangle \rangle} \\ &\times \sum_{H, c_H, H', c_{H'}} \kappa_{H'|H} \langle N_H \rangle b_{c_H} m_{c_H, h} \langle N_{H'} \rangle b_{c_{H'}} m_{c_{H'}, h'}. \end{aligned} \quad (15)$$

The normalization of the BF with decays included is

$$Z_{h'|h} = \frac{1}{4} \{K_{h'|h} - K_{h'|\bar{h}} + K_{\bar{h}'|h} - K_{\bar{h}'|\bar{h}}\}. \quad (16)$$

For use later on, a function is defined that is symmetric in h and h' :

$$\begin{aligned} W_{h'|h} &\equiv \frac{\langle \langle N_h \rangle \rangle}{\langle \langle N \rangle \rangle} K_{h'|h} = \left\{ \sum_{H, c_H} \frac{\langle n_H \rangle}{\langle n \rangle} b_{c_H} m_{c_H, h} m_{c_H, h'} + \sum_{H, c_H, H', c_{H'}} \frac{\langle n_H \rangle \langle n_{H'} \rangle}{\langle n \rangle^2} w_{H', H} b_{c_H} m_{c_H, h} b_{c_{H'}} m_{c_{H'}, h'} \right\}, \\ w_{H', H} &= [\langle n \rangle (q_{Ha} \chi_{ab}^{-1} q_{H'b})]. \end{aligned} \quad (17)$$

Here, $\langle n_H \rangle$ is the density of hadrons of species H and $\langle n \rangle$ is the net hadron density, at the time chemical equilibrium is lost. $\langle \langle N_h \rangle \rangle / \langle \langle N \rangle \rangle$ is the ratio of hadrons of type h to total hadrons in the final state,

$$\langle \langle N \rangle \rangle = \sum_h \langle \langle N_h \rangle \rangle. \quad (18)$$

IV. CALCULATING BFS FROM BLAST-WAVE MODEL

By inspection of the expression for $W_{h'|h}$ in Eq. (17) and the way in which it relates to $K_{h'|h}$ in Eq. (17), one can see that the BFS can be generated by a two step process. In the first step the contribution from decays, the first sum in Eq. (17), is calculated. This is performed by creating a hadron H at T_c , then emitting the descendants of H from the same point in coordinate space according to the blast-wave prescription. One increments the BF using all pairs of hadrons descending from the same original hadron H . In the second step, one calculates the correlation deriving from the preexisting correlation between two hadrons H and H' at T_c . One places all descendants of H at one point, and all descendants of H' at a second point. The two points are correlated in coordinate space according to parameters σ_R and σ_η . The preexisting correlation is then projected onto all pairs of particles involving one hadron from H and one from H' . Here, the species h' and h are typically chosen to be of opposite sign, so that the BF is positive represents the enhancement for finding an opposite charge. Examples are $\pi^+\pi^-$, K^+K^- , $p\bar{p}$, π^+K^- , $\pi^+\bar{p}$, and $K^+\bar{p}$. The BFS can be generated for specific species, $B_{h'|h}$, by following the method enumerated below.

- (1) Beginning with a list of hadrons, their masses, degeneracies, and charges, one calculates the charge susceptibility matrix at the temperature T_c , the last temperature for which chemical equilibrium was maintained. This involves calculating the density of each species, then using Eq. (10) which provides the susceptibility, or charge fluctuation, for a noninteracting hadron gas. Using that susceptibility, one calculates $W_{HH'}$ according to Eq. (17).
- (2) The contribution to the BF from decays, the first term in Eq. (17), is calculated using Monte Carlo sampling. First, a number of initial hadrons, N_{mc} , are generated. A species H is chosen proportional to $\langle n_H \rangle / \langle n \rangle$ which is calculated at temperature $T_c = 150$ MeV. All decay products of H with lifetimes less than 100 fm/c are then chosen according to the branching ratios. The decay products are then all placed in coordinate space at a position r according to the blast-wave prescription. That point is generated by first picking the transverse coordinates x and y according to a uniform distribution up to some radius R . That coordinate is then incremented by a random Gaussian step characterized by the parameter σ_R . For this contribution, the additional Gaussian step is chosen to maintain consistency with the second contribution described below. Once the position is known, the transverse velocity is given by the

blast-wave parameters U_\perp and R ,

$$u_x = U_\perp \frac{x}{R}, \quad u_y = U_\perp \frac{y}{R}. \quad (19)$$

Here, u_i refers to the relativistic velocity, $u_i = v_i / \sqrt{1 - v^2}$. Each product is then assigned a different momentum according to the final freeze-out temperature $T_f = 100$ MeV and collective flow $U_\perp = 1.092$ as described in the blast-wave description provided in Appendix A. Because of boost invariance, all particles can be placed at the position $z = 0$. Decays with lifetimes greater than 100 fm/c are then simulated. If any two species h and h' both appear in the final products, an array is incremented according to their relative momentum, rapidity, or azimuthal angle. The array represents the first term in function $W_{h'|h}$ in Eq. (17). It is binned by whichever kinematic variable is being considered, e.g., relative rapidity. One also increments a counter of N_h and $N_{h'}$. After sufficient sampling, the binning of $W_{h'|h}$ is translated into a binning of $Z_{h'|h}$ according to Eqs. (16) and (17), which involves dividing by a factor $\langle \langle N_h \rangle \rangle / \langle \langle N \rangle \rangle$. The array is also divided by N_{mc} . This then provides the contribution to $B_{h'|h}$ from decays. It should be emphasized that this contribution to decays does not accurately reproduce the invariant mass distribution because it assumes that all products of decays with lifetimes less than 100 fm/c rescatter. For example, in a more realistic model, some ρ mesons would decay into final state pions with neither pion rescattering. The relative rapidity or relative angle distributions of a ρ decay are not much different than those from rescattered products because the decay energy a ρ is similar to the thermal energy, but the difference would be more pronounced if binned by relative momentum. The contribution from decays where both products emerge unscathed is often considered part of the final-state interaction. For example, the K^+K^- outgoing wave function can be modified to include ϕ decays. Given that the focus here is mainly on how femtoscopic correlations distort charge balance functions, this approximate picture is sufficient.

- (3) The contribution to $B_{h'|h}$ from the second term in Eq. (17) is then calculated. This also is calculated with a Monte Carlo procedure. First, two particles are generated independently: species H and H' . They are chosen according to the thermal weights consistent with the temperature T_c . Decay products for each particle are then chosen according to the branching ratios. The transverse spatial coordinates are chosen by first picking a common point \vec{r} according to a uniform distribution in transverse coordinate space up to a radius R . From that point, two different points, one for the products h , of H , and the second for the products h' of H' are found by taking Gaussian random steps relative to \vec{r} . The steps in transverse space are characterized by σ_R , whereas the steps in spatial rapidity are characterized by σ_η . The two sets of particles are then generated close to one another, with the descendants of

H separated from the descendants of H' by an amount determined by σ_η and σ_R . Again, at this point decays with lifetimes greater than 100 fm/c are not yet performed. Any additional decays are then simulated. At this point, the momenta of particles descending from a single hadron as described in (1) are the same as those coming from either H or H' here. Along with the final momenta, the positions of the last interactions are stored for the purpose of calculating correlations from FSI. The array representing $W_{h'|h}$ is then incremented, but the array elements are not incremented by unity, but instead by $W_{HH'}$. Again, the array for N_h is incremented. Finally, the array is divided by N_{mc} and the factor $\langle\langle N_h \rangle\rangle / \langle\langle N \rangle\rangle$. Whereas the contribution described in (2) represents the correlation from the decays of a single hadron created at T_c , the contribution described in (3) represents how two hadrons that were correlated at the T_c project that correlation onto their descendants.

Finite acceptance is only crudely taken into account by ignoring any pairs with relative rapidity greater than $2Y_{\max}$, with $Y_{\max} = 0.9$, corresponding to the STAR acceptance. This ignores the p_t dependence of the acceptance and efficiency. Even if experiments were to correct for acceptance and efficiency, this calculation would be questionable due to the fact that low p_t particles are not measured and because the low p_t cutoff depends strongly on rapidity, especially for heavier particles. Much more realistic models of BFs have been constructed and analyzed, e.g., [4,25,26]. These more sophisticated treatments account for the difference between the distance scales over which strangeness, electric charge, or baryon number are conserved. Decays are more realistically taken into account and experimental acceptance and efficiency are considered in detail. More sophisticated treatments can lead to BF widths changing by a few tens of percent from the models used here. But the much simpler, much less numerically intensive model used here is sufficient to satisfy the goal of this study, which is to understand the degree to which FSI and BF correlations must be simultaneously considered. Comparison with experimental data is not the immediate goal of this study.

V. SCREENING FINAL-STATE COULOMB INTERACTIONS

Correlations from FSI can be calculated according to a number of methods, which tend to become equal when the relative momentum is small [32]. For larger relative momenta, the main method is to generate a pair of hadrons, independent of one another, with momentum \vec{p}_1 and \vec{p}_2 , from space-time coordinates x_1 and x_2 . One then increments a two-particle distribution by an amount $|\phi_{hh'}(\vec{q}, \vec{r})|^2$. The distribution is typically binned by relative momentum, but could be binned by some other variable such as relative rapidity. Here, \vec{q} and \vec{r} refer to the relative momentum and position in the center of mass of the pair. Because $q \neq 0$, the relative position depends on the time at which \vec{r} is calculated. Here, it is assigned the value corresponding to the separation of the two trajectories at a time halfway between the two emissions, and \vec{q} and \vec{r} are

calculated in the pair's rest frame. The correlation function is then the average of $|\phi|^2$ within each bin. This method provides a realization of Eq. (2).

The squared wave functions differ from unity due to the symmetrization or antisymmetrization of the wave functions, the strong interaction, and the Coulomb force between the two particles. Symmetrization and antisymmetrization effects are typically unimportant for $q \gtrsim 50$ MeV/c. Aside from resonant interactions, e.g., $\rho^0 \rightarrow \pi^+\pi^-$, the strong interaction is most manifest at small relative momentum due to the lack of competing phase space. Other resonant interactions certainly provide peaks, but those are usually considered within the context of charge balance correlations. Coulomb interactions are relatively weak in magnitude, but extend over larger relative momentum. For large q the squared wave functions can be considered classically [43], and when averaged over direction depend on q as

$$|\phi(\vec{q}, \vec{r})|^2 \approx 1.0 - \frac{2\mu z_1 z_2 e^2}{q^2 r}. \quad (20)$$

A classical expression also exists to account for the dependence on the angle between \vec{q} and \vec{r} [43], and is presented in Appendix B. The same- and opposite-sign correlation functions have oppositely signed contributions from Coulomb correlations. Thus, they reinforce one another when constructing a BF. For more central collisions, the correlation functions weaken due to the $1/r$ dependence above. However, when translating a correlation function to a BF, a factor of the multiplicity arises. The radii roughly scale as $(dN/dy)^{1/3}$, so the Coulomb contribution to the BF should increase with multiplicity, roughly as $(dN/dy)^{2/3}$. Thus, Coulomb effects might provide non-negligible contributions to the BF, even if their contribution to the correlation function is below a tenth of a percent.

If two charged particles, with momenta \vec{p}_a and \vec{p}_b and charges Z_a and Z_b , interact via the Coulomb interaction at large relative momenta, one can ask whether the interaction should be screened by the fact that both a and b are accompanied by balancing charges. For large relative momenta or large relative rapidity or large relative angle, particles are likely to be separated far in coordinate space because of the collective flow. For example, if two particles are separated by a unit of rapidity in momentum space, they were likely emitted from points separated by approximately one unit of spatial rapidity, i.e., separated by ≈ 20 fm at the breakup of the collision. In the limit that these separations are large, balancing charges should perfectly screen the Coulomb interaction, because particle b should see both a and the balancing charge of a . In [36] the screening effect was crudely estimated with a pion gas, and it was seen that without screening the Coulomb interaction noticeably distorted the BF, but that after accounting for screening the Coulomb effect only affected the first few bins of relative rapidity. Here, we improve on that picture by accounting for the fact that the balancing charges are spread across all species of particles. For example, the existence of a positive kaon not only promotes the existence of a negative kaon, but might also affect the number of pions, protons, or their antiparticles. Decays, which were neglected in the

previous study, are taken into account here. Finally, in this study distortions from FSI are also calculated for $p\bar{p}$ and K^+K^- BFs.

For the standard algorithm described above, an uncorrelated pair, a, b , is generated then weighted with $|\phi_{ab}(\vec{q}, \vec{r})|^2$. The two-particle distribution is then assigned a weight, which, if the particle did not interact, would be unity. To include screening, one must alter the weight to include the interaction with accompanying particles:

$$\begin{aligned} C_{ab} - 1 \approx & [|\phi_{ab}(\vec{q}_{ab}, \vec{r}_{ab})|^2 - 1] \\ & + \sum_{a'} K_{a'|a} [|\phi_{a'b}(\vec{q}_{a'b}, \vec{r}_{a'b})|^2 - 1] \\ & + \sum_{b'} K_{b'|b} [|\phi_{ab'}(\vec{q}_{ab'}, \vec{r}_{ab'})|^2 - 1] \\ & + \sum_{a'b'} K_{a'|a} K_{b'|b} [|\phi(\vec{q}_{a'b'}, \vec{r}_{a'b'})|^2 - 1]. \quad (21) \end{aligned}$$

This expression accounts for all the interactions between the particle a and its accompanying balancing cohort and between the particle b and its cohort. Final-state interactions within a cohort are ignored, aside from those that were responsible for the kernel K . For a given particle a there are many more particles in other cohorts than in the same cohort. The indices a, a', b, b' reference all the information of a specific particle including its type, momentum, and position. The usual Koonin equation would ignore the latter three terms in Eq. (21).

One might have chosen a different form for the correlation weight C_{ab} in Eq. (21). An obvious choice might be to take the product of the four wave functions rather than the sum. In the limit that the wave functions are near unity the choices become identical. For Coulomb or strong interactions, the variation of $|\phi_{ab}|^2$ from unity is indeed small except in a small region of phase space where $q_{ab} < 50$ MeV/ c , and the chance that for some sets of particles that multiple values of q are not small, the two choices should be similar. For identical particle interference, the form of $|\phi|^2$ could be $1 \pm \cos(qr)$. The oscillating piece is not small, but for most pairs qr is large and the oscillations simply provide noise. Thus, the final answer should not be significantly dependent on exactly how Eq. (21) is chosen.

When q_{ab} is large, weights are dominated by Coulomb interactions. In this case the kernel weights combined with the fact that the factors $[|\phi|^2 - 1]$, which are proportional to the ratios of charges, should lead to a cancellation. Physically, this can be considered as screening. If the particle b has a large relative momentum to a , one expects that the balancing cohort to a should cancel the interaction. In contrast, for small relative momentum a and b would spend significant time under one another's influence, and the effects of the cohorts should disappear.

To generate the correlations described by Eq. (21) one needs to sum over all hadron species a' and b' that accompany a and b . The particles a' are first generated according to their final yields, i.e. they are chosen with probability $p' = \langle \langle N_{h'} \rangle \rangle / \langle \langle N \rangle \rangle$. The positions of a and a' are chosen in a correlated manner in the same manner described for calculating BFs in Sec. IV. The additional weights, $W_{h'|h}$, defined in

Eq. (17) are used to modify the correlation weights in Eq. (21),

$$\begin{aligned} C'_{ab} - 1 \approx & [|\phi_{ab}(\vec{q}_{ab}, \vec{r}_{ab})|^2 - 1] \\ & + \sum_{a'} K_{a'|a} [|\phi_{a'b}(\vec{q}_{a'b}, \vec{r}_{a'b})|^2 - 1] W_{a'a} \\ & + \sum_{b'} K_{b'|b} [|\phi_{ab'}(\vec{q}_{ab'}, \vec{r}_{ab'})|^2 - 1] W_{b'b} \\ & + \sum_{a'b'} K_{a'|a} K_{b'|b} [|\phi(\vec{q}_{a'b'}, \vec{r}_{a'b'})|^2 - 1] W_{a'a} W_{b'b}. \quad (22) \end{aligned}$$

An array is calculated to represent the numerator of the correlation function. Based on the momenta of a and b the appropriate bin is chosen, then incremented by C'_{ab} . A separate array is used for the numerator, but it is incremented by unity. Finally, the correlation function is found by dividing the numerator's array by that of the denominator. The correlation for a given bin thus represents the average of C'_{ab} for pairs that fit that bin.

In some cases the particles a and b described above are unstable, i.e., they decay after being emitted from the fireball which is chosen for any decays with lifetimes greater than 100 fm/ c . This might include long-lived states like the η meson. In that case the weight C'_{ab} described above is used to increment the bins defined by any decay products of a with and decay products of b .

VI. RESULTS: DISTORTIONS TO BFs FROM FINAL-STATE INTERACTIONS

Femtoscopic correlation functions were first generated with the blast-wave model. Blast-wave parameters were chosen to fit the spectra and pion source sizes. The fitting procedure for choosing the blast-wave parameters is described in Appendix A. They were $T_c = 150$ MeV, $T_f = 100$ MeV, $U_\perp = 1.092$, $R = 13.4$ fm, and $\tau = 13.4$ fm/ c . It should be emphasized that the blast-wave model is crude. Fitting to blast-wave models tends to result in shorter breakup times than seen in much more realistic hybrid models which incorporate both a hydrodynamic stage and a microscopic hadronic simulation. However, these parameters do roughly reproduce both the spectra and like-sign pion femtoscopic correlations, so they are well suited for the purpose of this study, which is to gauge the importance of these effects in BF analyses. The parameters representing the spread of the charge correlation in coordinate space were set to $\sigma_\eta = 0.5$ and $\sigma_R = 3.0$ fm. These are defined in Sec. IV and in Appendix A. These last two parameters crudely reproduce experimental BFs, with the emphasis on being crude. The spread should be significantly broader for $p\bar{p}$ and K^+K^- BFs than for $\pi^+\pi^-$ BFs. The two spreads describe how balancing charges, which were already separated at chemical freeze-out, are separated at kinetic freeze-out. This separation encapsulates both the original separation at T_c and the additional spread during the hadron phase. In contrast, if two balancing particles come from the same decay during the hadron phase, their emission is assumed to occur at the same point. Even though this is a rather simple picture, a rough picture is sufficient for gauging

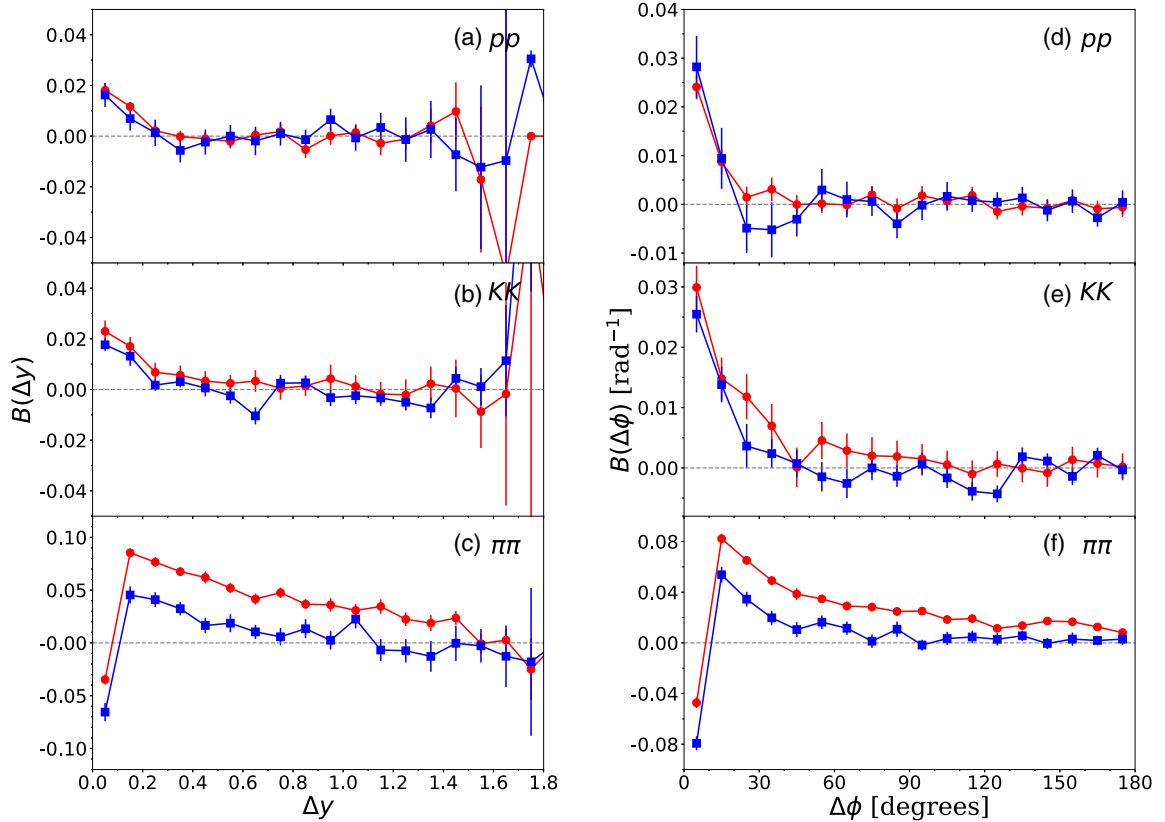


FIG. 1. Contributions to BF from femtosopic correlations are shown as a function of relative rapidity for (a) pp , (b) KK , and (c) $\pi\pi$. The kaon and proton BF are affected marginally, and only in the first two bins. The contribution never exceeds more than 0.02. The contributions to the $\pi\pi$ BF are more substantial and extend further in rapidity. The femtosopic contributions are displayed without (red circles) and with (blue squares) screening. The screening mainly affects results at larger relative rapidity, and significantly lowers the femtosopic contribution to the $\pi\pi$ BF. The right-side panels, (d)–(f), show the same behavior when binned by relative azimuthal angle.

the effect of femtosopic correlations on BF. The calculations presented here required a large amount of statistics due to the small size of the effect and the noise related to the inclusion of cross-correlations from balancing charges. The number of pairs generated for the calculations here exceeded 10^{12} , which would have made using a more sophisticated, and slower, model untenable.

Using the methods described in Sec. V, femtosopic correlations were calculated. To reduce noise in the femtosopic correlations below a tenth of percent, over 10^{12} pairs were analyzed. Because particles were sampled according to their multiplicities, correlations for kaons or protons were noisier than for pions. Figure 1 shows the contribution to BF from FSI. Calculations are displayed both with and without screening. For results without screening correlation functions were calculated using Koonin's equation, Eq. (2), which neglects how FSI between two particles affect correlations those other particles involved in balancing the charges of the first two. If not for screening, a non-negligible contribution would be present in the $\pi\pi$ BF, which would extend to larger relative rapidity or relative azimuthal angle. BF were generated by multiplying regular correlation functions by the multiplicity of uncorrelated particles in the same bins. Because pions have higher multiplicity, the effect on the BF was more noticeable. After the inclusion of screening the distortion to the BF are

only in the first few bins, at small relative rapidity or angle. For $\pi\pi$ the contributions in the first bin are negative due to the positive contribution from the same-sign correlation function due to identical-particle statistics. For slightly larger relative momentum, femtosopic effects are mainly from the Coulomb interaction. The Coulomb contribution to the correlation functions are negative for same-sign correlations and positive for opposite-sign correlations. The BF contribution, which is constructed by subtracting the same-sign correlation from the opposite-sign correlation, is positive.

To gain insight into whether the distortions to the BF from FSI are significant, the femtosopic contribution, with screening included, is added to the main contribution from charge balance. The calculation for the main charge balance is a rather crude model, and should not be taken seriously to better than 10–20%, but is sufficient for gauging the relative strength of the femtosopic contributions. Calculations of the BF with and without the femtosopic contributions are displayed in Fig. 2.

Figures 1 and 2 address the first questions posed for this study. BF are modified slightly, but noticeably, by femtosopic correlations. Those contributions are mainly in the first several bins of relative rapidity or relative azimuthal angle. Whereas the $\pi\pi$ BF are noticeably affected, albeit modestly, the modifications to the pp and KK BF are

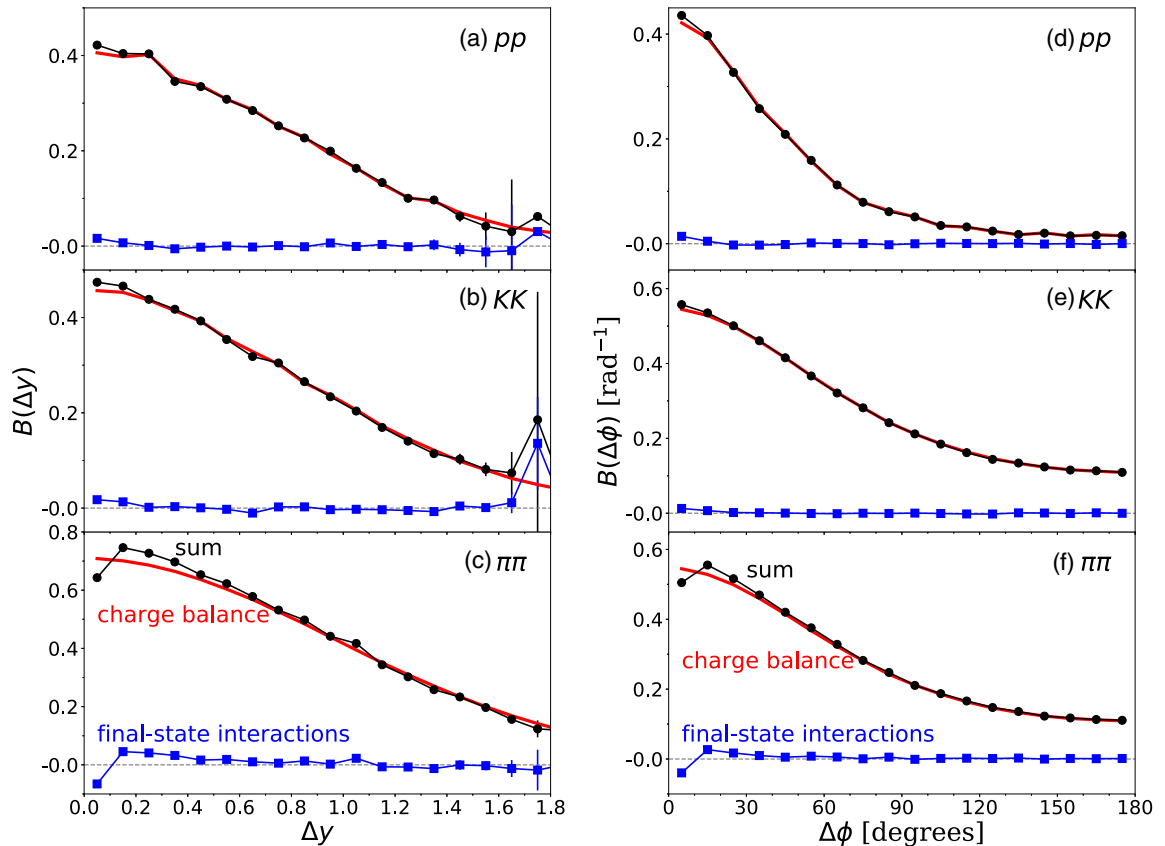


FIG. 2. The contribution to the BF (blue squares) is shown against the simple BF from local charge conservation only (red line), along with the sum of the two contributions (black circles). The effects of femtosopic correlations are modest, but noticeable, for the $\pi\pi$ BFs. The dip at small relative momentum derives from the positive correlation from identical-particle interference in the same-sign correlation functions. The slight positive correction is due to final-state Coulomb interactions. The same behavior is seen in BFs binned by relative rapidity (left-side panels) and relative azimuthal angle (right-side panels).

negligible. The Coulomb contribution to the femtosopic correlation functions are of similar magnitude for $\pi\pi$, KK , and pp correlations, but BFs involve multiplying correlations by the multiplicity of background pairs in a given bin, which is a significantly smaller factor for protons and kaons. Thus, it was not surprising that the effects are larger for $\pi\pi$ balance functions.

The shape of the modification for the $\pi\pi$ BF was also as expected as it was seen in [36]. The magnitude of the effect is reduced compared to the calculation in [36], but that calculation had ignored the effect of long-lived decays, which reduces the magnitude of the femtosopic correlation. The dip for the bins with lowest relative rapidity or angle was due to identical-particle interference for same-sign pions. The rise for the next few bins is due to the Coulomb interaction. As shown in Fig. 1 this part of the effect was significantly dampened by the inclusion of screening effects. The fact that each charge is accompanied by balancing charge of the opposite sign effectively screens the charge, unless the relative momentum is so small that the screening charges have little chance of standing between the charges of interest. If the calculations had been performed at lower beam energy, Coulomb effects would have been smaller. This is because Coulomb forces are long range and thus a given charge affects

a greater number of other charges when there are more charges present.

By accounting for the FSI weights of balancing particles, the distortions to the BFs from Coulomb effects are significantly muted. Further, by applying these weights to and from balancing partners, the correct normalization was restored. Even for FSI from identical particles, the normalization would have been incorrect if only the Koonin contribution to the BFs had been considered. For identical-particle statistics, symmetrization affects only those other pions within a similar bin of phase space, a number which is set by the local phase space density. Thus, if the average phase space density is 5%, there tends to be an overall enhancement of 0.05 to the area underneath the BF. If the calculations were repeated for less central collisions, the net contribution to the BF from symmetrization would be similar, but it would be spread out over larger relative momentum because larger source sizes lead to more extended correlation functions. The dip for small Δy and small $\Delta\phi$ would then be less pronounced.

One clear result of these calculations is that FSI distortions are nearly negligible for pp and KK BFs. This is important because those BFs play crucial roles in understanding the chemical evolution and diffusivity of the matter created in heavy-ion collisions.

VII. RESULTS: DISTORTIONS TO FEMTOSCOPIC CORRELATIONS FROM CHARGE-BALANCE CORRELATIONS

The effect of charge-balance correlations are typically neglected in calculations of correlations for femtosopic purposes. Here, we investigate the degree to which that is justified. First, femtosopic correlations were calculated from the blast-wave model as described in Appendix A. Correlations were found for both π^+ and π^- pairs. BFs were then calculated for the simple parametric model described in Appendix A. The difference between the like-sign and opposite-sign correlations from BFs is then

$$C_{\text{opp. sign}}(Q_{\text{inv}}) - C_{\text{same sign}}(Q_{\text{inv}}) = \frac{1}{dN_{\pi}/dQ_{\text{inv}}} B(Q_{\text{inv}}),$$

$$Q_{\text{inv}}^2 \equiv -(p_1 - p_2)^2. \quad (23)$$

Here, dN_{π}/dQ_{inv} is the number of pion pairs of the same sign separated by Q_{inv} divided by the number of pions of that same sign.

Figure 3 displays femtosopic correlations alongside those for BFs. The factor dN_{π}/dQ_{inv} scales as Q_{inv}^2 at low Q_{inv} due to phase space. For this reason the effect of charge balance is muted at low relative momentum, and the effect never rises above the half-percent level. This level of distortion is negligible given the current precision with which identical-pion femtoscopy is being analyzed. Because BFs are constructed by taking the difference between opposite-sign and like-sign correlations, it is difficult to assign that correlation specifically to either $C_{\text{same sign}}$ vs $C_{\text{opp. sign}}$. For charge balance from decays late in the reaction, one expects most of that strength to appear in the opposite-sign correlation. However, charge balance correlations from equilibrated systems, before final decays, tends to be split evenly between the opposite-sign and same-sign pieces if the systems are large [44,45]. Luckily, given that the contributions are so small, it does not matter what fraction of it should be assigned to the same-sign vs opposite-sign correlation functions.

The main lesson taken from Fig. 3 is that femtosopic analyses can safely ignore the contributions from charge balance for central heavy-ion collisions. For peripheral collisions or for pp collisions, the effects are probably non-negligible. For small source sizes femtosopic correlations can extend to $Q_{\text{inv}} \approx 200$ MeV/c and dN_{π}/dQ_{inv} can be small. Also, for small systems other classes of correlations also tend to interfere with the result, including momentum conservation. In fact, the validity of the Koonin equation comes into question when the overall source size is not much larger than the inverse characteristic momentum [32].

VIII. SUMMARY

BFs represent the best means for addressing questions about chemical evolution in high-energy heavy-ion collisions. In particular, one needs to evaluate the shape of the BF when binned by rapidity. If the quark chemistry is equilibrated within the first fm/c, balancing charges can separate by ≈ 1 unit of spatial rapidity by the time hadrons are finally emitted from the fireball. This is manifested by broad BFs, particu-

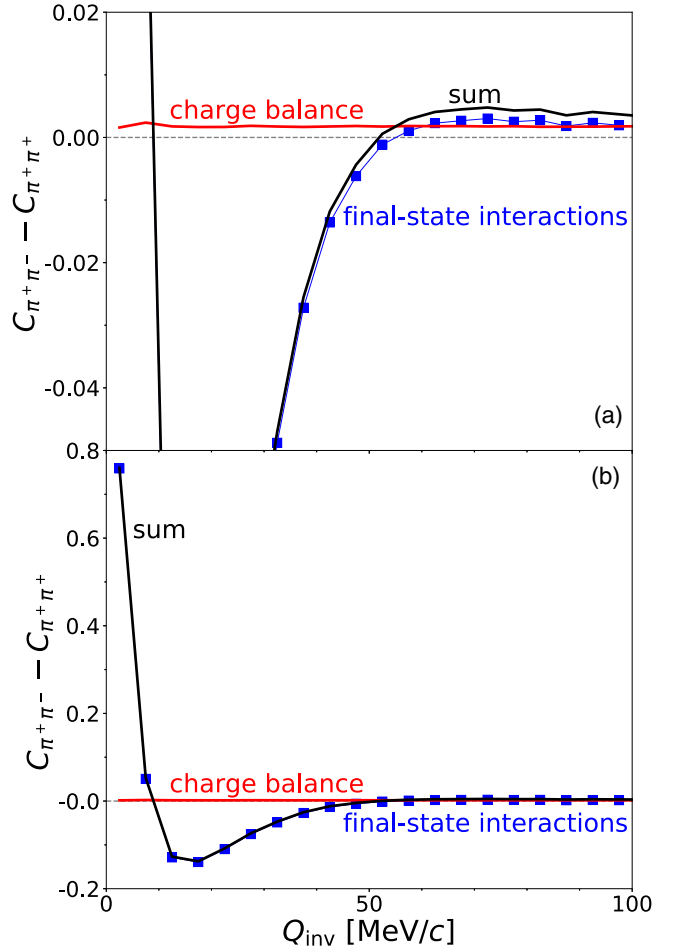


FIG. 3. The contribution of charge-balance effects (red line) is much smaller than the femtosopic correlation (blue squares) at small relative momentum. The net correlation is thus little changed. Because BFs provide the difference between opposite-sign and same-sign correlations, and, because the effect was small, only the difference between $C_{\text{opp. sign}}$ and $C_{\text{same sign}}$ correlations were analyzed. The same calculations are shown in both panels, with the vertical scale in panel (a) being magnified to show the size of the contribution from final-state interactions.

larly for K^+K^- and $p\bar{p}$ BFs. However, two other classes of phenomena also provide correlations that might potentially interfere with the interpretation of BFs. The first is correlation from final-state interactions, which represents the topic of this paper. The second is baryon-baryon annihilation, which is a topic for future study.

The contribution of femtosopic correlations, i.e., those from final-state interactions, was estimated in a previous study. But, for that study, only pions were considered, long-lived decays were neglected, and the distortions of BFs binned by relative azimuthal angle were not considered. Given the importance of the shapes of the K^+K^- and $p\bar{p}$ BFs, it was felt that a new study was needed. In the basic formulation, i.e. the, Koonin formula, femtosopic correlations enhance the emission of like-sign pions due to the symmetrization of the two-particle outgoing wave function. This provides a negative contribution to the BF. Coulomb effects enhance the emission

of opposite-sign pairs, whereas they discourage the emission of same-sign pairs. For pp or $p\bar{p}$ pairs, a resonant-like interaction at small relative momentum enhances the emission of same-sign pairs. However, the net integral of the BF must be unchanged, because for every extra particle of a given charge there must exist exactly one extra particle of the opposite sign, regardless of FSI. If the emission of same-signed pairs is enhanced by some effect then the emission of opposite-sign pairs must also be correspondingly enhanced to maintain the strict requirement of global charge conservation.

The issues described in the previous paragraph motivated the current study. An ambitious model was developed where additional weight from final-state interactions was applied not only to the interacting pair, but to any balancing partners. This required modeling how each charge particle was accompanied by additional particles. For each charged particle a of hadron type h , a probability was found for it to be accompanied by a hadron of type h' . The additional hadron a' was then placed in vicinity of a according to a parametric form of the correlation. The charge-balance arguments from Sec. III show how one can consider a' as being any hadron, then applying a balancing weight $w(a'|a)$ based on charge balance. The weight $w(a'|a)$ takes into account charge balance at the point of chemical equilibrium and decays to determine how the weight depends on the specific species a and a' . The correlation of a and a' in momentum space was crudely modeled by assuming a simple correlation in coordinate space that is mapped onto momentum space via a blast-wave model. In addition to parameters to set the temperature and flow velocity, the blast-wave model had parameters describing how the emission points of a and a' would be correlated in coordinate space. If one is considering the interaction weight of pion a with pion b , one must also apply that weight to all the balancing partners of a , i.e. those denoted by a' , with b and all its balancing partners of b' . Because the charge of the balancing partners a' exactly cancel those of a , the interaction weight for a and b is also applied to opposite sign pairs, albeit spread over a wider range of relative momentum. This preserves the charge conservation constraint of the BF in a way that more realistically accounts for how balancing charge is spread amongst different species at different locations. Additionally, weights were projected through the chain of decays occurring between a point where chemical occurred and when the particles are emitted. This rather long-winded procedure is especially necessary for Coulomb interactions. Once a particle b is separated from a by larger relative momentum, it is as likely to feel the interactions with the balancing particle a' as it is to be influenced by a . Thus, the balancing charge effectively screens the Coulomb effects for larger relative momentum.

The approach and methods described and developed herein were then applied to calculating the femtoscopic contributions to $\pi^+\pi^-$, K^+K^- , and $p\bar{p}$ BFs. Significant effects were only found for the $\pi^+\pi^-$ case. Although the effect on correlation functions is of similar strength for all three cases, the translation to BFs involves a factor of the multiplicity, which is higher for pions than for kaons or protons. The contribution to the $\pi^+\pi^-$ BF was confined to the first few bins in relative rapidity or azimuthal angle, but would have extended further if screening effects had not been included. The size of the

correction for conditions similar to central collisions of Au+Au at RHIC were modest and somewhat smaller than what was found with the simpler model considered in [36].

The main conclusions of the study are that

- (1) Femtoscopic correlations should provide a modest dip in the $\pi^+\pi^-$ BF at small relative rapidity or relative azimuthal angle, followed by a small enhancement at slightly larger values.
- (2) For K^+K^- or $p\bar{p}$ BFs, the effect of correlations from final-state interactions is negligible.
- (3) Correlation functions at small relative momentum used for femtoscopic purposes based on final-state interactions can safely neglect the influence of charge-conservation effects, at least for central heavy-ion collisions.

These findings are reassuring. They validate the practice of treating femtoscopic and charge-balance effects separately, although one might wish to apply a small FSI correction to $\pi^+\pi^-$ BFs. The rather crude nature of the modeling here, especially the use of a blast wave, should predict this additional structure to the $\approx 10\%$ level, but given that the distorting effects are at the five percent level, calculating the distortion of a 5% effect to ten percent accuracy should be sufficient to add the corrections from a simple model to BF calculations from more sophisticated models.

As mentioned earlier, there is an additional effect that might also complicate the interpretation of BFs. Baryon annihilation depletes the pp BF at smaller relative momentum, relative rapidity or relative angle. Combined with this study, a detailed estimate of how annihilation affects BFs should enable the confident interpretation of experimental BFs. This is crucial if BFs are to provide a quantitative and rigorous means for extracting information about the chemistry and diffusivity of matter created in relativistic heavy-ion collisions.

ACKNOWLEDGMENTS

This work was supported by the Department of Energy Office of Science through Grant No. DE-FG02-03ER41259 and by the National Science Foundation's CSSI Program under Award No. 2004601 (BAND Collaboration). The authors are grateful for the assistance with fitting routines provided by Ozge Surer.

APPENDIX A: BLAST-WAVE MODEL

Charge conservation correlates balancing particles in coordinate space. The correlation is then projected onto momentum space through collective flow. A blast-wave model provides a simple parametric means to describe final-state collective flow. For this study, a particularly simple blast-wave prescription is applied. More complicated prescriptions, that take into account phenomena such as elliptic flow, exist [46]. In Bjorken coordinates [47], particles are all emitted at a fixed proper time τ_f . This is the time measured by an observer moving with a constant velocity from the $z = 0$ plane at time $t = 0$ to the emission point. In terms of the laboratory time t

and the longitudinal coordinate z ,

$$\tau = \sqrt{t^2 - z^2}. \quad (\text{A1})$$

In terms of spatial rapidity,

$$\eta_s = \frac{1}{2} \ln \left(\frac{t+z}{t-z} \right), \quad (\text{A2})$$

emission is given a Gaussian distribution corresponding to the finite rapidity range of emission at RHIC,

$$dN/d\eta_s \sim e^{-\eta_s^2/2\Sigma_\eta^2}, \quad (\text{A3})$$

with $\Sigma_\eta = 1.8$.

The distribution of emission points in the transverse plane is considered a constant up to some maximum radius, R . The momenta is determined by a temperature T_f and a transverse collective velocity parametrized by u_\perp ,

$$u_i = u_\perp \frac{r}{R}. \quad (\text{A4})$$

Here, u_i represents the component of the four-velocity, $u_i = v_i/\sqrt{1-v^2}$. Along the beam axis the collective velocity is chosen to equal the spatial rapidity, $y = \eta_s = \sinh^{-1}(u_z)$. Particles were generated stochastically. Final yields were scaled to reproduce the experimental number, so the blast-wave model only serves as a means to assign momenta and space-time coordinates to the momenta. Species were chosen proportional to the multiplicity at the time of emission, $\langle\langle N_h \rangle\rangle$. This multiplicity was determined by first generating particles proportional to their densities in an equilibrated system at temperature $T_c = 150$, corresponding to the densities latest time at which chemical equilibrium might have been maintained, $\langle n_h \rangle$. Particles were then decayed according to their branching ratios. All decays with lifetimes less than 100 fm/c were simulated. The products were then randomly placed in the blast-wave volume and assigned momenta consistent with the final blast-wave temperature and collective velocity. Any further decay was simulated. We thus have

$$\langle\langle N_h \rangle\rangle = \sum_{H, c_H} \langle N_H \rangle b_{c_H} m_{c_H, h}, \quad (\text{A5})$$

where b_{c_H} is the branching ratio for a particular channel c_H and $m_{c_H, h}$ is the number of hadrons of type h in that channel. This prescription does ignore the fact that some short-lived particles, like Δ baryons or ρ mesons, might still exist at the final breakup. Though the number of such resonances should be significantly fewer as compared to the earlier equilibrium, regeneration would suggest that a number of such resonances would be emitted at the final time with all the decay products escaping rescattering. But this should have little effect on spectra because most of the resonances are rather broad so that the final momenta differ only slightly compared to being rethermalized. Further, because the lifetimes are short, femtoscopic correlations are not strongly affected.

Blast-wave parameters T_f , R , τ_f , and U_\perp were reproduced through comparison of simulated models with experimental data from 200A GeV Au+Au collisions at RHIC. For the spectra calculations MCMC generated hadrons were used to construct spectra, which were then compared to experimental

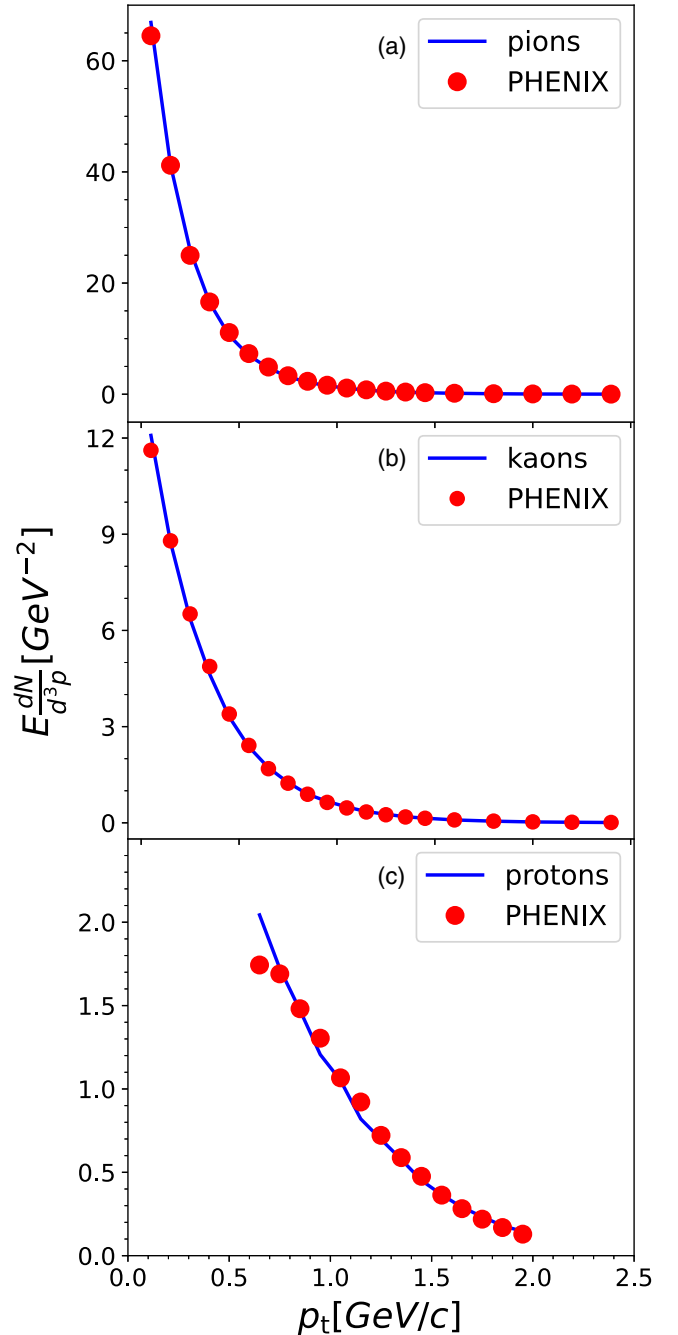


FIG. 4. Spectra for pions, kaons, and protons are compared to experimental results for central (0–5% centrality) collisions of 200A GeV Au+Au collisions as a function of transverse momentum. Model results (blue lines) roughly match PHENIX results (red circles).

data from the PHENIX Collaboration [48]. A χ -square minimization using the software describe in [49] was applied to obtain the most likely parameters, which are listed in Sec. VII. Fits are shown in Fig. 4 for kaons, protons, and pions. Modeling spectra produced a fit of the parameters T_f and U_\perp which were consequently utilized in the calculation of correlations to evaluate the final two parameters, the transverse size R and the freeze-out time τ_f . To generate the correlation functions,

values of τ_f and R were used to generate CFs using the Koonin prescription. CFs were then compared to experimental data from same-sign two-pion correlations functions measured by the STAR Collaboration [50]. The same minimization used to fit the spectra was utilized to minimize the difference between data and experiment while varying the parameters of interest, with the best fit illustrated in Fig. 5. The final parameter values are mentioned in Sec. VII.

APPENDIX B: CLASSICAL EXPRESSIONS FOR THE SQUARED COULOMB WAVE FUNCTION

Here, we provide a slightly different form of the expressions derived in [43]. The relation between the squared outgoing wave function and classical trajectories is

$$\begin{aligned} |\phi(q, r, \cos \theta)|_{\text{classical}}^2 &= \left| \frac{d^3 q_0}{d^3 q}(q, r, \cos \theta) \right| \\ &= \frac{q_0}{q} \left| \frac{d \cos \theta_0}{d \cos \theta} \right|. \end{aligned} \quad (\text{B1})$$

Here, \vec{q} is the asymptotic relative momentum whereas \vec{q}_0 is the relative momentum at the time of emission, when the separation was \vec{r} . The angle θ is between the vectors \vec{q} and \vec{r} . Energy conservation, $q^2/2\mu = q_0^2/2\mu + Z_1 Z_2 e^2/r$, or equivalently $q dq = q_0 dq_0$, was used to simplify the expression. Thus, $|\phi|_{\text{classical}}^2$ describes how a phase space element $d^3 q_0$ is focused into $d^3 q$.

To calculate the Jacobian, we consider a particle of mass μ at position $\vec{r} = r\hat{z}$ has an initial direction defined by θ_0 and a final direction described by θ . From [43] one can see that conservations of angular momentum, energy, and the Lenz vector allow one to express $\cos \theta_0$ in terms of $\cos \theta$:

$$\begin{aligned} \cos \theta_0 &= \frac{q}{q_0} \cos \theta - \frac{q}{2q_0} \frac{\epsilon}{(1 \pm \sqrt{1 - 2\epsilon/(1 + \cos \theta)})}, \\ \frac{q_0}{q} &= \sqrt{1 - \epsilon}, \quad \epsilon = \frac{Z_1 Z_2 e^2/r}{q^2/2\mu}. \end{aligned} \quad (\text{B2})$$

Thus, $\cos \theta_0$ can be expressed solely in terms of $\cos \theta$ and ϵ , the ratio of the initial Coulomb energy to the total energy in the center-of-mass frame. For when the charges have opposite sign, the interaction is attractive and $\epsilon < 0$, whereas $\epsilon > 0$ for same-sign pairs.

Calculating $d \cos \theta_0/d \cos \theta$ and applying Eq. (B1) then gives the ‘‘classical’’ squared wave function,

$$\begin{aligned} |\phi(q, r, \cos \theta)|_{\text{classical}}^2 &= \sum_{\pm} 1 \pm \frac{1}{\beta} \left[\frac{\epsilon}{(1 \pm \beta)(1 + \cos \theta)} \right]^2, \\ \beta &= \sqrt{1 - \frac{2\epsilon}{1 + \cos \theta}}. \end{aligned} \quad (\text{B3})$$

There are two solutions to the trajectories, because there are two initial angles that can reproduce a given final angle. To understand the relation for $|\phi|_{\text{classical}}^2$ it is useful to view the relationship between $\cos \theta$ and $\cos \theta_0$, which are illustrated for the attractive and repulsive cases in Fig. 6. For the repulsive case, there are final angles which are unreachable, because the Coulomb force diverts those trajectories with

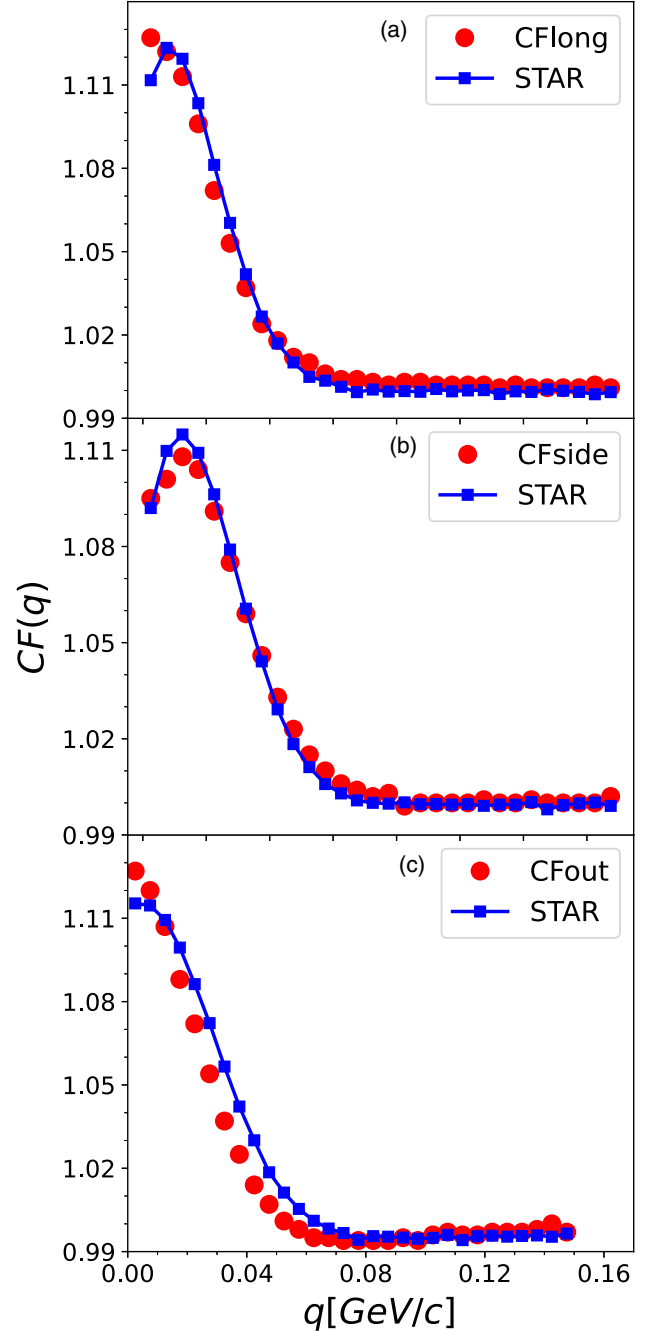


FIG. 5. Two-pion correlation function projections as a function of relative momentum are shown for the model (blue lines) fit to data from the STAR Collaboration (red circles). Measurements are from 200A GeV Au+Au collisions in the 0–5% percent centrality range. The three projections are for relative momentum along the beam axis (‘‘CFlong’’), parallel to the pair momentum in the longitudinal comoving frame (‘‘CFout’’), and perpendicular to both the pair momentum and the beam axis (‘‘CFside’’).

$\cos \theta_0$ near -1.0 . In both cases, there are points for which $d \cos \theta_0/d \cos \theta$ are divergent, but these divergences are integrable. Even though there are divergences as $|\phi|_{\text{classical}}^2 \rightarrow \infty$ for the repulsive case, if one averages $|\phi|_{\text{classical}}^2$ over $\cos \theta$, the

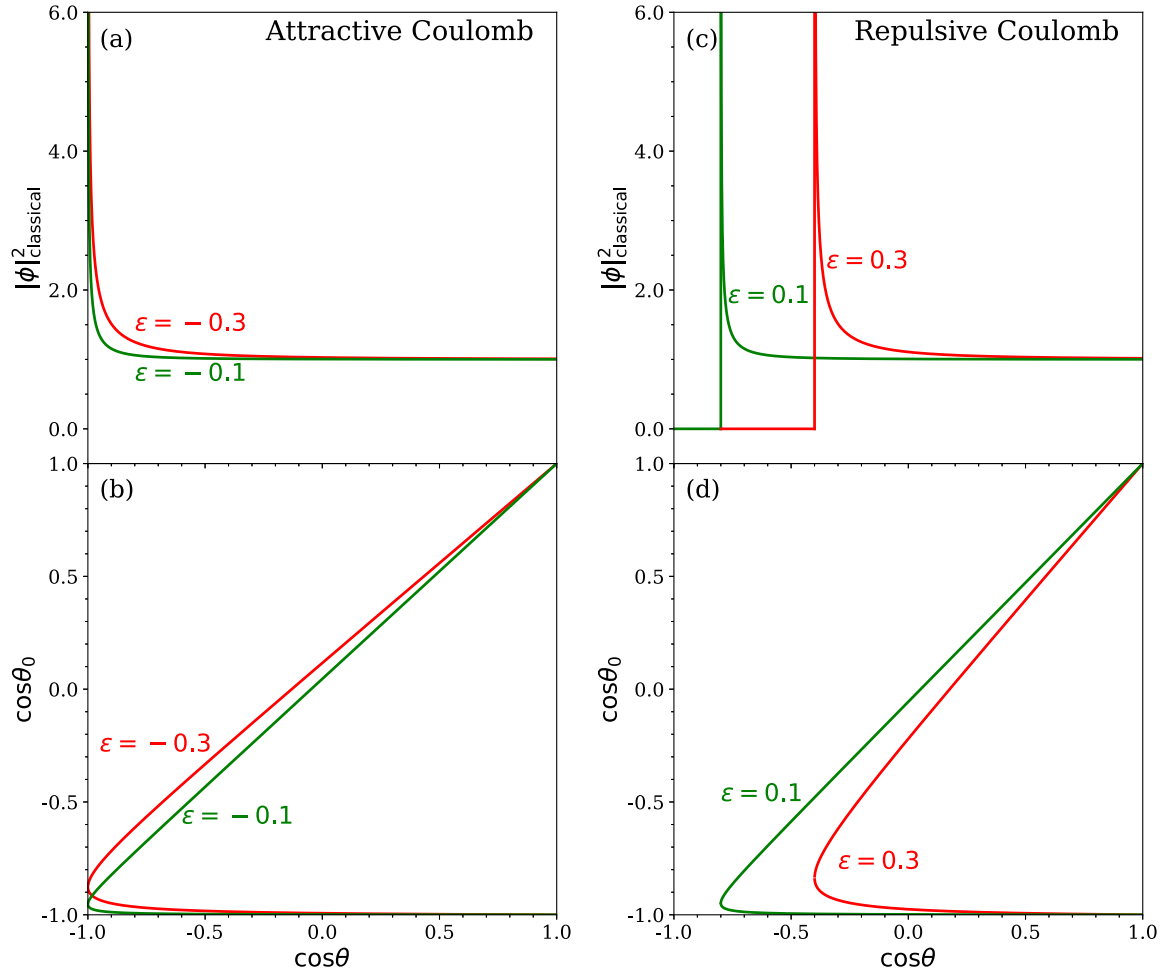


FIG. 6. For large relative momenta classical expressions are applied for the squared relative wave functions. The classical analogy of the squared wave functions are generated from the relation between the final direction of the relative momenta and the initial direction. This is illustrated in the lower panels of both figures where angles are relative to the original relative position. Because the squared wave function depends on the Jacobian, $d \cos \theta_0 / d \cos \theta$, there are integrable poles in the wave function. The effective squared wave function, $|\phi|^2$, depends on the final direction θ and on the ratio of the original potential energy, $Z_1 Z_2 e^2 / r$, to the final relative energy, $q^2 / 2\mu$.

result is below unity and

$$\frac{1}{2} \int d \cos \theta |\phi(\epsilon, \cos \theta)|_{\text{classical}}^2 = \frac{q_0}{q} = \sqrt{1 - \epsilon} \quad (\text{B4})$$

for both the attractive and repulsive cases.

When applying classical approximations for the wave function in Koonin's formula, one should be mindful of the

divergences shown in Fig. 6. They are integrable, and the expressions remain tenable in a Monte Carlo sampling procedure given sufficient sampling. However, the divergences do bring along a good deal of noise, even for the small values of ϵ used in the studies here. In the cases studied here, where the classical expressions are only applied for $q > 500 \text{ MeV}/c$, typical values of ϵ are ≈ 0.001 .

-
- [1] S. A. Bass, P. Danielewicz, and S. Pratt, *Phys. Rev. Lett.* **85**, 2689 (2000).
 [2] S. Pratt, W. P. McCormack, and C. Ratti, *Phys. Rev. C* **92**, 064905 (2015).
 [3] S. Pratt, *Phys. Rev. Lett.* **108**, 212301 (2012).
 [4] S. Pratt and C. Plumberg, *Phys. Rev. C* **102**, 044909 (2020).
 [5] G. D. Westfall (STAR Collaboration), *Acta Phys. Hung. A* **21**, 249 (2004).
 [6] L. Adamczyk *et al.* (STAR Collaboration), *Phys. Rev. C* **94**, 024909 (2016).
 [7] H. Wang (STAR Collaboration), *J. Phys. G* **38**, 124188 (2011).
 [8] H. Wang (STAR Collaboration), *J. Phys.: Conf. Ser.* **316**, 012021 (2011).
 [9] N. Li *et al.* (STAR Collaboration), *Indian J. Phys.* **85**, 923 (2011).
 [10] M. M. Aggarwal *et al.* (STAR Collaboration), *Phys. Rev. C* **82**, 024905 (2010).
 [11] G. D. Westfall (STAR Collaboration), *J. Phys. G* **30**, S345 (2004).

- [12] J. Adams *et al.* (STAR Collaboration), *Phys. Rev. Lett.* **90**, 172301 (2003).
- [13] H. Wang, Ph.D. thesis, Michigan State University, 2012 (unpublished).
- [14] B. I. Abelev *et al.* (STAR Collaboration), *Phys. Lett. B* **690**, 239 (2010).
- [15] S. Acharya *et al.* (ALICE Collaboration), [arXiv:2110.06566](https://arxiv.org/abs/2110.06566).
- [16] J. Pan (ALICE Collaboration), *Nucl. Phys. A* **982**, 315 (2019).
- [17] S. N. Alam (ALICE Collaboration), PoS **EPS-HEP2017**, 151 (2017).
- [18] M. Weber (ALICE Collaboration), PoS **EPS-HEP2013**, 200 (2013).
- [19] B. I. Abelev *et al.* (ALICE Collaboration), *Phys. Lett. B* **723**, 267 (2013).
- [20] M. Weber (ALICE Collaboration), *Nucl. Phys. A* **904-905**, 467c (2013).
- [21] J. Pan, Ph.D. thesis, Wayne State University, 2019, https://digitalcommons.wayne.edu/oa_dissertations/2305/
- [22] C. Alt *et al.* (NA49 Collaboration), *Phys. Rev. C* **71**, 034903 (2005).
- [23] C. Alt *et al.* (NA49 Collaboration), *Phys. Rev. C* **76**, 024914 (2007).
- [24] S. Pratt, J. Kim, and C. Plumberg, *Phys. Rev. C* **98**, 014904 (2018).
- [25] S. Pratt and C. Plumberg, *Phys. Rev. C* **99**, 044916 (2019).
- [26] S. Pratt and C. Plumberg, *Phys. Rev. C* **104**, 014906 (2021).
- [27] S. Borsanyi, Z. Fodor, S. D. Katz, S. Krieg, C. Ratti, and K. Szabo, *J. High Energy Phys.* **01** (2012) 138.
- [28] G. Aarts, C. Allton, A. Amato, P. Giudice, S. Hands, and J. I. Skullerud, *J. High Energy Phys.* **02** (2015) 186.
- [29] A. Amato, G. Aarts, C. Allton, P. Giudice, S. Hands, and J. I. Skullerud, *Phys. Rev. Lett.* **111**, 172001 (2013).
- [30] S. E. Koonin, *Phys. Lett. B* **70**, 43 (1977).
- [31] M. A. Lisa, S. Pratt, R. Soltz, and U. Wiedemann, *Annu. Rev. Nucl. Part. Sci.* **55**, 357 (2005).
- [32] S. Pratt, *Phys. Rev. C* **56**, 1095 (1997).
- [33] S. Pratt, *Phys. Rev. D* **33**, 1314 (1986).
- [34] S. Pratt, E. Sangaline, P. Sorensen, and H. Wang, *Phys. Rev. Lett.* **114**, 202301 (2015).
- [35] S. Pratt, *Phys. Rev. Lett.* **53**, 1219 (1984).
- [36] S. Pratt and S. Cheng, *Phys. Rev. C* **68**, 014907 (2003).
- [37] H. P. Zbroszczyk (STAR Collaboration), PoS **WPCF2011**, 006 (2011).
- [38] A. Kisiel, *Nukleonika* **49**, s81 (2004).
- [39] R. Rapp and E. V. Shuryak, *Nucl. Phys. A* **698**, 587 (2002).
- [40] Y. Pan and S. Pratt, *Phys. Rev. C* **89**, 044911 (2014).
- [41] J. Steinheimer, J. Aichelin, M. Bleicher, and H. Stöcker, *Phys. Rev. C* **95**, 064902 (2017).
- [42] O. Savchuk, V. Vovchenko, V. Koch, J. Steinheimer, and H. Stoecker, *Phys. Lett. B* **827**, 136983 (2022).
- [43] Y. D. Kim, R. T. de Souza, C. K. Gelbke, W. G. Gong, and S. Pratt, *Phys. Rev. C* **45**, 387 (1992).
- [44] S. Pratt and R. Steinhorst, *Phys. Rev. C* **102**, 064906 (2020).
- [45] O. Savchuk, R. V. Poberezhnyuk, V. Vovchenko, and M. I. Gorenstein, *Phys. Rev. C* **101**, 024917 (2020).
- [46] F. Retiere and M. A. Lisa, *Phys. Rev. C* **70**, 044907 (2004).
- [47] J. D. Bjorken, *Phys. Rev. D* **27**, 140 (1983).
- [48] A. Adare *et al.* (PHENIX Collaboration), *Phys. Rev. C* **88**, 024906 (2013).
- [49] P. Virtanen, R. Gommers, T. E. Oliphant, M. Haberland, T. Reddy, D. Cournapeau, E. Burovski, P. Peterson, W. Weckesser, and J. Bright *et al.*, *Nat. Methods* **17**, 261 (2020).
- [50] J. Adams *et al.* (STAR Collaboration), *Phys. Rev. C* **71**, 044906 (2005).